Chemical Engineering Journal 388 (2020) 124176

Contents lists available at ScienceDirect

Chemical Engineering Journal

journal homepage: www.elsevier.com/locate/cej

Influence of temperature and other system parameters on microbial fuel cell performance: Numerical and experimental investigation

Siddharth Gadkari[a,b,*], Jean-Marie Fontmorin[c], Eileen Yu[c], Jhuma Sadhukhan[a,b]

[a] Centre for Environment and Sustainability, University of Surrey, Guildford, Surrey GU2 7XH, United Kingdom
[b] Department of Chemical and Process Engineering, University of Surrey, Guildford GU2 7XH, United Kingdom
[c] School of Engineering, Newcastle University, Newcastle Upon Tyne, United Kingdom

HIGHLIGHTS

- Steady state 2D mathematical model of an air-cathode MFC is developed.
- The nonlinear effect of temperature on MFC performance is investigated.
- Model accounts for energy balance in addition to the mass and charge balance.
- Effect of local current density and reaction rate on MFC performance is studied.
- Model can be used for parametric analysis and optimization studies.

ARTICLE INFO

Keywords:
Microbial fuel cell
Temperature
Mathematical model
Electrode spacing
Ionic strength
Bioelectrochemical systems

ABSTRACT

This study presents a steady state, two dimensional mathematical model of microbial fuel cells (MFCs) developed by coupling mass, charge and energy balance with the bioelectrochemical reactions. The model parameters are estimated and validated using experimental results obtained from five air-cathode MFCs operated at different temperatures. Model analysis correctly predicts the nonlinear performance trend of MFCs with temperatures ranging between 20 °C and 40 °C. The two dimensional distribution allows the computation of local current density and reaction rates in the biofilm, helping to correctly capture the interdependence of system variables and predict the drop in power density at higher temperatures. Model applicability for parametric analysis and process optimization is further highlighted by studying the effect of electrode spacing and ionic strength on MFC performance.

1. Introduction

A microbial fuel cell (MFC) uses the growth and metabolic activities of microorganisms (such as exoelectrogenic bacteria) to directly convert the chemical energy in organic wastes to electricity [1]. Air-cathode MFCs in particular have been extensively researched for efficient power generation, as they help avert the need to aerate the water for the oxygen reduction reaction (ORR) at the cathode [2–4]. The bioelectrochemical system designed to make the energy transfer possible in an MFC involves a complex interplay between standard electrochemical kinetics and transport phenomena (fluid flow, mass & energy transfer) with biologically catalysed redox reactions [5,6]. As one would assume, the involvement of microorganisms adds to the complexity and also significantly increases the number of variables that affect the performance of these systems. In order to design efficient MFCs for electricity production and reduction of the effluent chemical oxygen demand in wastewater, the effect of the different parameters on the MFC performance must be better understood [5,7–9].

One important parameter for MFCs is the operating temperature. It has been shown that temperature has a strong influence on many variables such as the conductivity of substrate solution (or wastewater), diffusion coefficient, charge transfer rates, activation energy, biochemical processes of the microbial communities, etc., the combined effect of which can significantly alter the MFC power output [6,10]. And while there have been some studies to understand the effect of temperature, there is no consensus [4,11–18].

Liu et al. [4] used an air-cathode MFC with acetate as the substrate and observed a 9% decrease in maximum power density when the MFC operating temperature was reduced from 32 °C to 20 °C. This decrease was mainly attributed to the corresponding reduction in cathode potential. Moon et al. [11] investigated the effect of temperature on the performance of a “Sensor-type” two chamber MFC fed with artificial

* Corresponding author at: Centre for Environment and Sustainability, University of Surrey, Guildford, Surrey GU2 7XH, United Kingdom.

https://doi.org/10.1016/j.cej.2020.124176
Received 19 July 2019; Received in revised form 10 January 2020; Accepted 19 January 2020
Available online 03 February 2020

wastewater (AW) and observed a rather nonlinear trend. The power output of MFC showed a slight increase as temperature was raised from 24 °C to 35 °C, but showed a decrease at higher temperatures, 38 °C and 41 °C. This nonlinear behaviour was associated with the changes in ohmic overvoltage [11]. Feng et al. [12] used full-strength beer brewery wastewater in an air-cathode MFC and observed a 17% decrease in power output when temperature was decreased from 30 °C to 20 °C. Their analysis showed that the primary reasons for the decrease was mainly the reduced performance of the cathodic reaction and not so much the biological effects at the (bio) anode [12].

Patil et al. [13] showed that the performance of the biofilms at any specific operation temperature is a strong function of the original incubation temperature during initial biofilm growth.They also showed that irrespective of the incubation temperature, bioelectrocatalytic steady state current densities decrease for operating temperatures above 40 °C, except for biofilms incubated at 35 °C, which show growth in performance with temperatures as high as 45 °C.

Min et al. [14] used a two-chamber MFC with domestic wastewater mixed with acetate as the substrate and observed ~34% decrease in maximum power density as the operating temperature was reduced from 32 °C to 20 °C. This is starkly different from the 9% decrease observed by Liu et al. [4] in the same temperature range, and can be mainly ascribed to the different MFC configurations and the type of substrate used. It should be noted that Min et al. observed no successful operation for MFC operated at 15 °C. So overall they predicted a continuous reduction in performance with decrease in temperature. Di Lorenzo et al. [15] and Larrosa-Guerrero et al. [16] both used single chamber MFC with air-cathode and also observed a reduction in power output as temperature was decreased from 30 °C to 20 °C and 35 °C to 4 °C respectively. It should be pointed out that the MFC studied by Larrosa-Guerrero et al. [16] did show power production (although relatively small) at low temperatures of 4 °C, 8 °C and 15 °C as opposed to the study by Min et al. [14] where the MFC failed to operate even at 15 °C.

Li et al. [17] used a two chamber MFC separated by a PEM and investigated the effect of temperature over a broad range of temperature from 10 °C to 55 °C. Li et al. observed results very similar to that of Moon et al., with the highest power density achieved at 37 °C, which decreased by 21% when temperature was raised to 43 °C. At the highest temperature 55 °C, no steady power generation was observed.

Given the complex interaction of temperature with other variables of the system, it is important to accurately quantify these variations and study local changes in the biofilm and the reaction chamber at different temperatures, something which is difficult with experiments but can be performed in a directed way using mathematical models [19–23]. One of the very few numerical studies where the effect of temperature on MFC was studied is the one by Oliveira et al. [24]. They coupled the heat, charge and mass balances with the bioelectrochemical reactions in the MFC to develop a one-dimensional steady state mathematical model. This computational study predicted a simple linear increase in power density as temperature was increased from 20 °C to 30 °C and then 40 °C [24]. However the results were not corroborated with any experimental data and are not in accordance with the results observed by Moon et al. [11] and Li et al. [17] at temperatures above 37 °C.

In this work, we have developed a 2D mathematical model to better quantify the process-parameter relationships and obtain a deeper insight on the effect of temperature on MFC performance. The model predictions are validated using experimental results based on a single chamber MFC with air-cathode. Effect of electrode spacing and ionic strength is also studied to highlight the broader applicability of the mathematical model.

2. Material and methods

2.1. Electrodes preparation

1.3 cm × 1.5 cm (1.95 cm^2 projected surface) flame-oxidized stainless steel (FO-SS) fiber felts were used as anode and 25 cm^2 Pt/C-modified carbon paper were used as GDEs. SS Fibre Felt (BZ40D, thickness 0.4 mm) was purchased from Xi'an Filter Metals Materials Co., Ltd (Shaanxi, China). Its mean pore size is 28.9 μm and porosity is 78 ± 5%. SS electrodes were first sonicated in acetone and ethanol for 15 min, thoroughly rinsed with distilled water and dried prior utilization. FO-SS electrodes were prepared as described in a previous study [25]. Briefly, oxidation of SS was conducted using the blue flame of a Bunsen burner fed with natural gas. Each side of the electrode was oxidized for about 30 s before being rinsed and dried. Carbon paper with gas diffusion layer (GDL) was purchased from Quintech (H2315 I2 C6, Göppingen, Germany) and further coated with 0.5 $mg\,cm^{-2}$ Pt/C to be used as GDE.

2.2. MFC reactors and operation

Four identical single-chamber membraneless air-cathode MFCs were constructed using Perspex®. The working volume of the anode chamber was 60 mL. The anolyte medium consisted of 0.05 M phosphate buffer pH 7.2, 280 mg L^{-1} NH_4Cl, 5.7 mg L^{-1} $CaCl_2$,$2H_2O$, 100 mg L^{-1} $MgSO_4$,$7H_2O$ and some micronutrients and vitamins detailed elsewhere [26]. 1000 $mg\,L^{-1}$ sodium acetate was used as sole carbon source. Reactors were inoculated with 20% v/v effluent from a parent MFC fed with glucose/glutamic acid and were operated in the dark at controlled temperature of 30 °C during the enrichment period. Ag/AgCl reference electrodes were used to monitor anode potentials and all MFCs cell voltages and anode potentials were monitored using an ADC-24 Picolog data logger (Pico Technology, Cambridgeshire, U.K.). Reactors were operated in batch and media were changed when cell voltages would drop. It was assumed that mature bioanodes were developed after 3 stable consecutive cycles were obtained. Polarisation tests were always carried out at the peak cell potentials (typically 15–18 h after media were changed) at different temperatures by first disconnecting external resistances for 30 min, before recording open circuit voltages (OCVs). External resistance values were then decreased and cell voltages were recorded 20 min after resistances were changed. The resistance values used were 102500, 10073, 2004, 1000, 750, 500, 400, 300, 200, 100, 50 and 25 Ω. Values obtained from polarisation tests were used to plot polarisation curves (power density vs. current density).

2.3. Numerical methods and calculations

The air-cathode membraneless MFC is modeled using a steady state two dimensional model, coupling bioelectrochemical kinetics with mass, charge and heat transfer. Schematic of the modeling domain is presented in Fig. 1.

The biofilm is assumed to be present on either side of the anode and is modeled here as a porous conductive matrix [27–29]. The anolyte can permeate the porous matrix where the bacteria oxidize the substrate to release electrons and hydrogen ions.

The mathematical model is based on the following assumptions:

- Biofilm is made up of a solid porous conductive matrix, with a fixed conductivity, σ_{bio}.
- pH is strictly controlled.
- Substrate is assumed to be ideally mixed in the anolyte and substrate gradient only exists in the biofilm.
- A concentration boundary layer exists between the biofilm matrix and the anolyte, and exhibits linear concentration profiles.
- Microbial population in the biofilm of the anode is uniformly distributed.

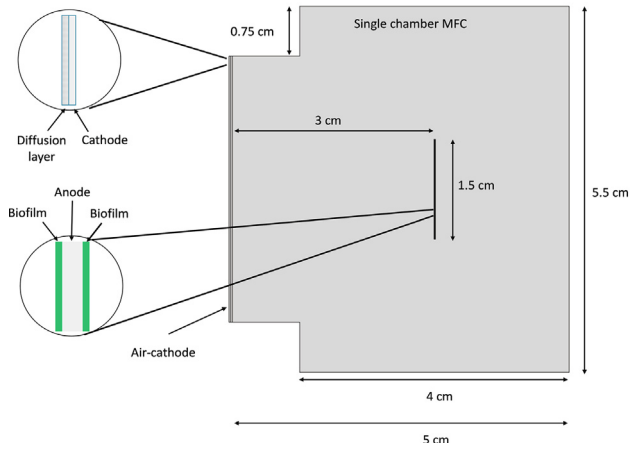

Fig. 1. Schematic of the 2D model domain of the singe chamber MFC with air cathode. Small sections of the anode and cathode are zoomed out to show the details.

- Equilibrium has been reached between microbial growth, decay and washout, maintaining a steady-state biofilm of fixed thickness.
- Acetate and CO_2 remain in the anode chamber and do not diffuse to the cathode assembly. Similarly air does not diffuse in the anodic chamber.
- Acetate is the only electron donor substrate in the anolyte.

The analysis assumes the following oxidation and reduction reactions at anode and cathode respectively:

$$(CH_2O)_2 + 2H_2O \rightarrow 2CO_2 + 8H^+ + 8e^- \quad (1)$$

$$O_2 + 4H^+ + 4e^- \rightarrow 2H_2O \quad (2)$$

2.3.1. Ohm's law and charge transfer kinetics

As described above, the biofilm is assumed to be a porous matrix capable of conducting electrons generated through substrate oxidation to the anode. A porous electrode is typically characterized by distinct electrode and electrolyte phases. In the biofilm matrix, the biomass components (made up of bacteria, the extracellular polymeric substances (EPS) and nanowires) are the solid conducting phase. The liquid anolyte (substrate solution) enters the porous biofilm matrix where the substrate is oxidized by the bacteria. The biofilm matrix works as a porous electrode and can be characterized by two separate current balances, one for the solid phase and one for the liquid electrolyte phase [30].

The transfer of electrons in the solid phase and the transfer of ions (protons in this case) in the electrolyte phase, both are governed by Ohm's Law.

$$I = \sigma \nabla \varphi \quad (3)$$

$$i = \nabla I \quad (4)$$

where, I is the current density, σ is conductivity, φ is potential and i is the current source term.

The specific current generation due to electrons and ions in case of porous electrode is expressed as follows:

$$i_s = \nabla I_s = \nabla(\sigma_{s,\text{eff}} \nabla \varphi_s) \quad (5)$$

$$i_l = \nabla I_l = \nabla(\sigma_{l,\text{eff}} \nabla \varphi_l) \quad (6)$$

where, the subscripts s and l refer to the electrode phase and electrolyte phase respectively. The effective values of conductivity (σ_{eff}) for the two phases are calculated based on Bruggeman model:

$$\sigma_{s,\text{eff}} = \epsilon_s^{1.5}\, \sigma_s \quad (7)$$

$$\sigma_{l,\text{eff}} = \epsilon_l^{1.5}\, \sigma_l \quad (8)$$

where, ϵ_s and ϵ_l represent the volume fraction of the electrode and electrolyte phase respectively.

Current density in the porous biofilm matrix is a function of substrate concentration, biomass concentration and overpotential (which can be derived from Butler–Volmer equation). Assuming substrate consumption by bacteria is governed by Monod kinetics, the charge transfer kinetics at anode can be described as in Eq. 9 [31,30].

$$i_a = i_{0,a} \left(\frac{C_s}{C_s + K_{s_a}} \right) C_x \ \exp\left(\frac{\alpha_a F \eta}{RT} \right) \quad (9)$$

where, C_s is concentration of the substrate, K_{s_a} is half max-rate substrate concentration, C_x is the anodophilic bacteria concentration, α_a is anodic transfer coefficient, F is Faraday's constant, η is overpotential, R is ideal gas constant, T is temperature, $i_{0,a}$ is the forward rate constant of anode reaction at standard conditions.

The air-cathode used in the microbial fuel cell is a gas diffusion electrode (GDE), a special type of porous electrode which in addition to the catalyst/electrode layer also contains a gas pore phase (gas diffusion layer, GDL) that is inert to charge transfer. Air (mixture of oxygen, nitrogen and water vapor) diffuses through the GDL to the catalyst/electrode layer where oxygen is reduced to produce H_2O.

The current density at the cathode can be described using concentration dependent Butler-Volmer equation, as in Eq. 10.

$$i_c = i_{0,c} \left(\exp\left[\frac{\alpha_c F \eta}{RT} \right] - \frac{C_{O_2}}{C_{O_2,\text{ref}}} \exp\left[\frac{-(1-\alpha_c) F \eta}{RT} \right] \right) \quad (10)$$

where, $i_{0,c}$ is the cathode reference exchange current density, C_{O_2} is the concentration of O_2, $C_{O_2,\text{ref}}$ is the reference concentration of O_2, α_c cathodic transfer coefficient.

The overpotential (η) is a function of electrode potential, electrolyte potential and the equilibrium potential of the charge transfer reaction at the particular electrode (E_{eq}) and is described as in Eq. 11.

$$\eta = \varphi_s - \varphi_l - E_{\text{eq}} \quad (11)$$

2.3.2. Mass transport of substrate in the biofilm

Substrate is assumed to be completely mixed in the anolyte solution. Gradient of substrate in the biofilm is expressed as is Eq. 12.

$$\nabla(D_{\text{eff,a}} \nabla C_s) = \frac{a_a i_a}{nF} \quad (12)$$

where, $D_{\text{eff,a}}$ is the effective diffusion coefficient, a_a is active specific surface area of anode, $n(=8)$is the number of electrons involved in acetate (substrate) oxidation.

As substrate cannot penetrate the solid anode, no-flux boundary condition (Eq. 13) is applied at the interface of the biofilm with the anode.

$$0 = D_{\text{eff,a}} \nabla C_s \quad (13)$$

Flux continuity condition (Eq. 14) is applied at the interface of the outer surfaces of the biofilm with the anolyte, assuming a concentration boundary layer of thickness 'L' at the interface.

$$\frac{D_a}{L}(C_{s,\text{bulk}} - C_s) = D_{\text{eff,a}} \nabla C_s \quad (14)$$

where, $C_{s,\text{bulk}}$ is the concentration and D_a is the diffusion coefficient of the substrate in the bulk anolyte.

2.3.3. Mass transport at air-cathode

Mass transfer of air (consisting of oxygen, nitrogen and water) through the GDE (cathode) is expressed using the mixture-averaged diffusion model (Eq. 15):

$$0 = -\nabla \cdot (\rho D_i^m \nabla \omega_i) + R_i \quad (15)$$

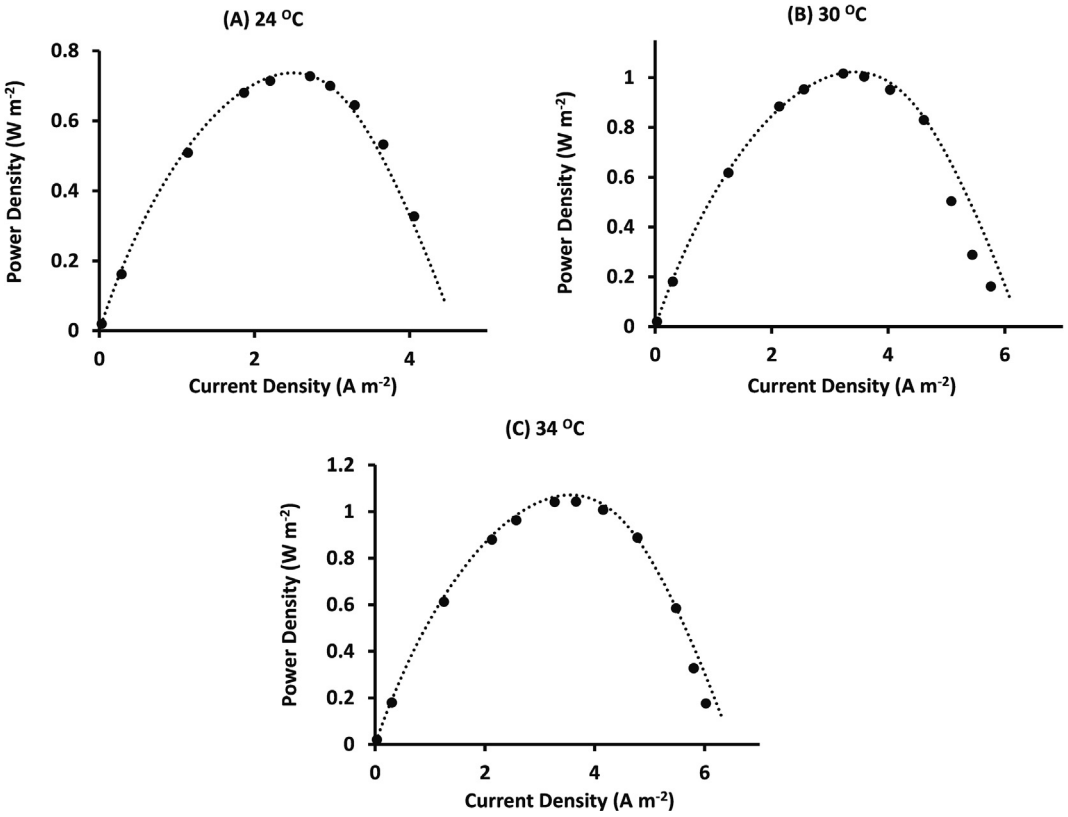

Fig. 2. Comparison of polarization curves (power density vs current density) obtained from experimental data (solid black circles) and numerical fitting (dotted line) for MFCs operating at (A) 24 °C, (B) 30 °C and (C) 34 °C.

here,

$$D_i^m = \frac{1-\omega_i}{\sum_{k\neq i}^{M} \frac{x_k}{D_{e_{ik}}}} \tag{16}$$

$$D_{e_{ik}} = \frac{\epsilon_{p,c}}{\tau_F} D_{i,k} \tag{17}$$

$$x_k = \frac{\omega_k}{M_k} M \tag{18}$$

$$\frac{1}{M} = \sum_{i=1}^{q} \frac{\omega_i}{M_i} \tag{19}$$

where, the subscript i refers to the different chemical species (O_2, N_2 and H_2O), ω refers to mass fraction, ρ denotes the mixture density, $\epsilon_{p,c}$ porosity of the GDE, D_i^m refers to mixture-averaged diffusion coefficient, $D_{i,k}$ refers to multicomponent Maxwell-Stefan diffusivities, $D_{e_{ik}}$ refers to effective multicomponent Maxwell-Stefan diffusivities, x_k refers to mole fraction of species k, M is the mean molar mass, τ_F is the fluid tortuosity factor ($=\epsilon_{p,c}^{-1/3}$, based on Millington and Quirk model [32]).

Reaction rates of the different species (R_i) are only applied in the catalyst/electrode layer.

$$R_{O_2} = -\frac{a_c i_c}{4F} \tag{20}$$

$$R_{H_2O} = \frac{2a_c i_c}{4F} = \frac{a_c i_c}{2F} \tag{21}$$

$$R_{N_2} = 0 \tag{22}$$

where a_c is the active specific surface area of cathode.

Air is assumed to be constantly present at the open boundary where the diffusion layer of the cathode assembly is exposed. Thus constant mass fractions of O_2, H_2O and N_2 are maintained at the open boundary (Eq. 23):

$$\omega_i = \omega_{i,0} \tag{23}$$

It is assumed that air does not pass into the anodic chamber, thus a no flux condition (Eq. 24) is applied at all boundaries expect the open boundary exposed to air.

$$n\cdot\left(\rho D_i^m \nabla\omega_i + \rho\omega_i D_i^m \frac{\nabla M}{M}\right) = 0 \tag{24}$$

2.3.4. Heat transport

Heat is generated in the microbial fuel cell due to the irreversible activation losses and the voltage losses during charge transport in the electrolyte and the solid conducting materials.

The steady state governing equation for heat transport in the MFC for the 2D model, is given as in Eq. 25:

$$0 = \nabla\cdot(d_z\, k\, \nabla T) + d_z\, Q_h \tag{25}$$

where, d_z is the thickness of the MFC in the z-direction (the component perpendicular to the 2D domain), k is the thermal conductivity and Q_h is the heat source.

In the porous electrodes, an effective conductivity, k_{eff}, is calculated based on solid (k_s) and electrolyte (k_l) conductivities as follows:

$$k_{\text{eff}} = \epsilon_s\ k_s + \epsilon_p\ k_l \tag{26}$$

The total heat source (Q_h) is a combination of Joule heating due to charge transport ($Q_{j,h}$) and the heat generated due to the electrochemical reactions (Q_r), and are defined as in Eqs. (27)–(29):

$$Q_h = Q_{j,h} + a_r\, Q_r \tag{27}$$

$$Q_{j,h} = -(i_s\cdot\nabla\phi_s + i_l\cdot\nabla\phi_l) \tag{28}$$

$$Q_r = (\phi_s - \phi_l - E_{eq,r})i_r \quad (29)$$

where the subscript r refers to either, a, for anode or, c, for cathode.

2.4. Parameter estimation and model validation

Experiments were performed for MFC's operating at five different temperatures, 20 °C, 24 °C, 30 °C, 34 °C, and 40 °C. Model parameters were estimated by using the experimental data at 24 °C, 30 °C and 34 °C. Applicability and accuracy of the predicted model parameters was later established by comparing the experimental data for other two MFCs, operating at 20 °C and 40 °C with numerical predictions.

Parameter estimation:

PDE solver, COMSOL, capable of handling coupled physics [33] was used for solving the numerical model. Best-fit regression analysis based on Nelder-mead simplex optimization method was used to determine the model parameters [19]. The objective function was defined as the difference between theoretical and measured power density values as a function of current density. Fig. 2 shows the experimental and fitted polarization curves for MFCs operating at 24 °C, 30 °C and 34 °C. As can be seen the numerical technique produced excellent fitting with experimental results. The resulting parameter values obtained from the curve fitting, and other parameters that were directly obtained from literature are provided in the Supplementary file.

Validation: To prove the model applicability over a broader range of temperatures than those that were used for parameter estimation, the model was used to predict the power density of MFCs operating at temperatures above and below of what were used for numerical fitting. Figs. 3A and 3B show the comparison of polarization curves between those obtained from the experimental study and numerical prediction for MFCs operating at 20 °C and 40 °C respectively.

As can be seen, there is fairly good agreement between predicted and experimental results, thus confirming the applicability of the mathematical model over a wide range of temperatures. It should be noted that the model is able to predict the nonlinear trend of power density as a function of temperature. It is observed from the experimental study that the maximum power density of MFCs for different operating temperatures increases linearly between 20 °C to 34 °C, however on further increase in operating temperature the power density begins to decrease. This change in trend was captured in the numerical results (Figs. 3A and 3 and further discussion on such decrease in performance at higher temperatures is presented in the results and discussion section.

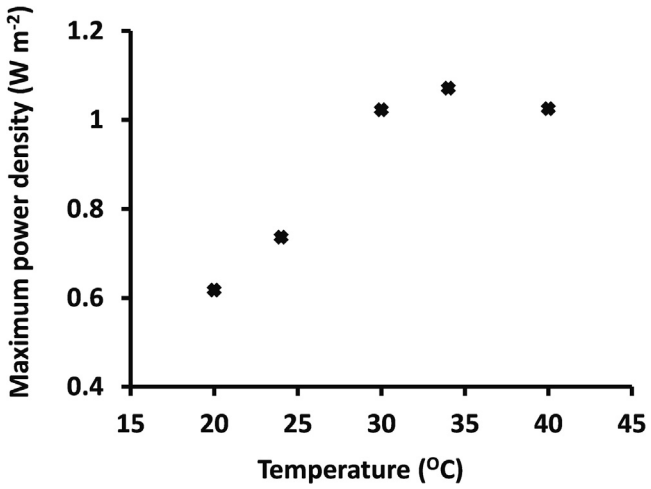

Fig. 4. Maximum power density as a function of temperature, as obtained from the experimental study.

3. Results and discussion

3.1. Effect of Temperature

Both the experimental results and the numerical predictions obtained in this study, as described in Section 2.4 above, have shown ~4.5% decrease in maximum power density for operating temperature of 40 °C compared to 34 °C (as shown in Fig. 4). This behaviour was a deviation from the consistent increase in power output obtained when the operating temperature was increased from 20 °C to 34 °C.

Some studies in the past have investigated the influence of temperature on MFC performance [4,12,14,13,15,16,11,17]. For example, Liu et al. [4], Feng et al. [12] and Min et al. [14], all observed a linear increase in power output as the temperature was increased from 20 °C to 32 °C, 20 °C to 30 °C and 22 °C to 30 °C in their respective studies. Larrosa-Guerrero et al. [16] also observed a similar increasing trend in power density as operating temperature of single chamber MFCs was moved up from 4 °C and 35 °C. It should be noted that in all the above studies the maximum operating temperature is up to 35 °C. And the performance trend of MFCs between 20 °C and 34 °C, obtained from the current study is in accordance with the above studies.

Few studies that have investigated MFC behaviour at higher temperatures have found a nonlinear performance trend, similar to the one observed in this work for operating temperature of 40 °C [11,13,17]. For example, Moon et al. [11] observed an improvement in MFC performance as the temperature was increased from 24 °C to 35 °C, however they observed a decrease in power density at higher temperatures

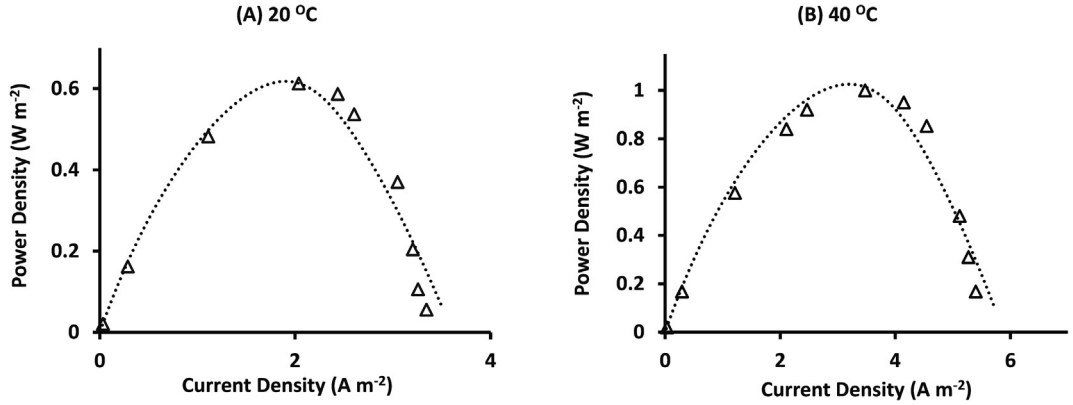

Fig. 3. Comparison of polarization curves (power density vs current density) obtained from experimental data with those predicted from the numerical simulations for MFCs operating at 20 °C and 40 °C. The open triangles represent the experimental data whereas the dotted line represents numerical prediction.

of 38 °C and 41 °C. Similarly Li et al. [17] have also observed a decrease in power density as the temperature was increased from 37 °C to 43 °C, while the same MFC system showed a linear trend when temperature was moved up from 10 °C to 37 °C [17]. It is postulated that the performance of microbial communities is compromised at temperatures above 37 °C which results in reduced efficiency [17].

Patil et al. [13] observed a decrease in current density when the operating temperature was raised above 40 °C, for MFCs using microbial biofilms that were grown at 22 °C and 27 °C incubation temperatures. However for biofilms incubated at 35°C, the linear trend between current density and temperature continued until 45 °C and decreased only when the operating temperature was raised beyond 45 °C. In the current work, all biofilms were incubated at 30°C, and effect of incubation temperature was not studied separately. However the general trend of decreased performance at higher temperatures (close to 40 °C and above) is still valid. As previously described, the numerical results from the 1D model developed by Oliveira et al. [24], fails to capture the nonlinear performance trend of MFC with temperature and predicted a rather linear increase in power density as temperature was increased from 20 °C to 40 °C.

To understand this non-linearity which is introduced at higher temperatures, we looked at the electrolyte current density (ECD) distribution in the MFC chambers for all five operating temperatures, which are described in Figs. 5B-5F. The current vector field (arrow plot), describing the direction of ion movements in the MFC chamber is shown in Fig. 5A. The ECD distribution plots highlight the different regions of low and high current density in the MFC chamber, with the highest being close to the anode and surrounding biofilms while the lowest for all temperatures is near the wall of the chamber farthest from the cathode. As can be seen from Figs. 5B-5F, maximum ECD for a given operating temperature, shows a linear increase from $5.2x10^{-2}$ Am^{-2} at T = 20 °C to $8.9x10^{-2}$ Am^{-2} at T = 34 °C. However on further increase in operating temperature, like at T = 40 °C, though the ECD distribution remains almost similar to that for T = 34 °C, the maximum ECD shows a small drop (~6%) to $8.4x10^{-2}$ Am^{-2}. The ECD essentially reaches a plateau for operating temperatures ⩾30 °C, as can be seen in the distribution plots shown in Figs. 5D, 5E and 5F.

Another important factor that governs the power generated in an MFC is the rate of substrate oxidation in the biofilm. To understand how this factor was affected, the reaction rate of oxidation in the biofilms is averaged and plotted as a function of temperature, as shown in Fig. 6. As can be seen, the average reaction rate shows a linear increase with temperature until T = 30°, after which it reaches a plateau and slowly begins to decrease. The maximum reaction rate of 52.84 mol m^{-3} d^{-1} is obtained for operating temperature of 34 °C, and it drops by about 7% to 49.11 mol m^{-3} d^{-1} for MFC operated at 40 °C.

The mathematical model and the estimated parameters effectively capture the postulated influence of temperature on conductivity (Ohmic resistance) and the bacterial activity in temperature dependent correlations of current density and other variables in the system, which provide the correct estimation of ECD & reaction rates and help predict the nonlinear performance trend. Together the electrolyte current density and the reaction rate of oxidation, result in the stagnation of maximum power density as operating temperature reaches 30° and the subsequent decline at T = 40° after showing a peak at T = 34°.

The composition of the culture and the substrate used in different MFCs, along with the specific configuration of the electrodes, together would determine the optimum temperature that can provide the highest power output without affecting the system efficiency. The proposed steady state model is generic and computationally efficient allowing fast convergence. It can be used for different MFC configurations for performing quick estimation (optimization) of 'ideal' temperature range of operation for a given combination of bacterial culture and substrates.

Fig. 7 shows the polarization plot (cell voltage [mV] vs current density [Am^{-2}]) and average cell temperature [°C] as a function of current density for MFC operating at 30 °C. As can be seen, cell voltage decreases from 680 mV to 20 mV as current density is increased from 0 to 6 Am^{-2}. On the other hand, average cell temperature has a linear relationship with current density and increases from 29.85 °C to 32.24 °C in the same interval. Though there is an increase in average temperature, it is quite low (~8%) and may not lead to any significant change in performance of the MFC. This suggests that the power dissipated from the electrochemical reactions at the two electrodes does not lead to any significant heat generation, which is expected considering the small current densities in MFC systems.

3.2. Effect of other system parameters on MFC performance

Along with temperature, several other design and operational parameters affect the MFC performance including the ionic strength, electrode spacing, type of bacterial culture in anode biofilm, substrate composition and its concentration, etc [6]. Thus a direct correlation between power density and temperature cannot be obtained unless all other parameters have been accounted. This necessitates the use of numerical modeling for effective optimization of MFC systems.

While the current steady state model, which couples energy balance with other physics is used for understanding the effect of temperature, it is also suitable for studying the influence of other systems parameters. The scope and applicability of the model is established by studying the change in power density as a function of ionic strength of the substrate solution and inter-electrode distance. The effect of these two parameters on the MFC performance is quite well-understood and the trends predicted from the model are compared with those described in literature.

3.2.1. Ionic strength

Fig. 8 shows the effect of ionic strength of the substrate solution (represented here as the electrolyte conductivity, σ_l) on the MFC performance. As can be seen from Fig. 8A, maximum power density initially increases linearly with increase in the electrolyte conductivity, as it goes up from 0.11 W m^{-2} at $\sigma_l = 1e^{-4}$ Sm^{-1} to 1.02 W m^{-2} for $\sigma_l = 1e^{-2}$ Sm^{-1}. However on further increase in conductivity, the corresponding growth in power density slows down and reaches a plateau as σ_l is increased to $2e^{-1}$ Sm^{-1}.

Conductivity of the solution determines the rate of ion transfer. Thus a higher conductivity improves ionic conduction and reduces the Ohmic losses, which thereby results in an improved power output from the MFC. The trend observed here is in accordance with many experimental studies in literature who have reported a similar upsurge in power density with increase in the ionic strength of the substrate medium and subsequent saturation after which increase in conductivity does not result in any further improvement in power density [4,14,30,34–36]. Also, it can be seen from Fig. 8B, the average reaction rate of substrate oxidation in the biofilm shows a similar trend as maximum power density with increasing electrolyte conductivity. The improvement in reaction rate with conductivity is result of direct manifestation of improved electrode potential due to reduction in Ohmic losses.

Conductivity of the solution is typically increased by adding NaCl or high concentration of buffer solution [4,12]. However very high salinity has also been reported to have a negative influence on the bacterial performance [37,35] and thus system sensitivity (specific to the type of microbial communities in the biofilm) should be carefully considered before adding any components to improve the ionic strength of the solution for improved performance.

3.2.2. Inter-electrode distance or electrode spacing

Fig. 9 shows the effect of inter-electrode distance (IED) between anode and cathode (also referred to as electrode spacing) on the MFC performance. IED was varied from 1 cm to 4 cm and as it can be seen from Fig. 9A, maximum power density increases as the distance between the two electrodes is decreased. The trend observed here is in

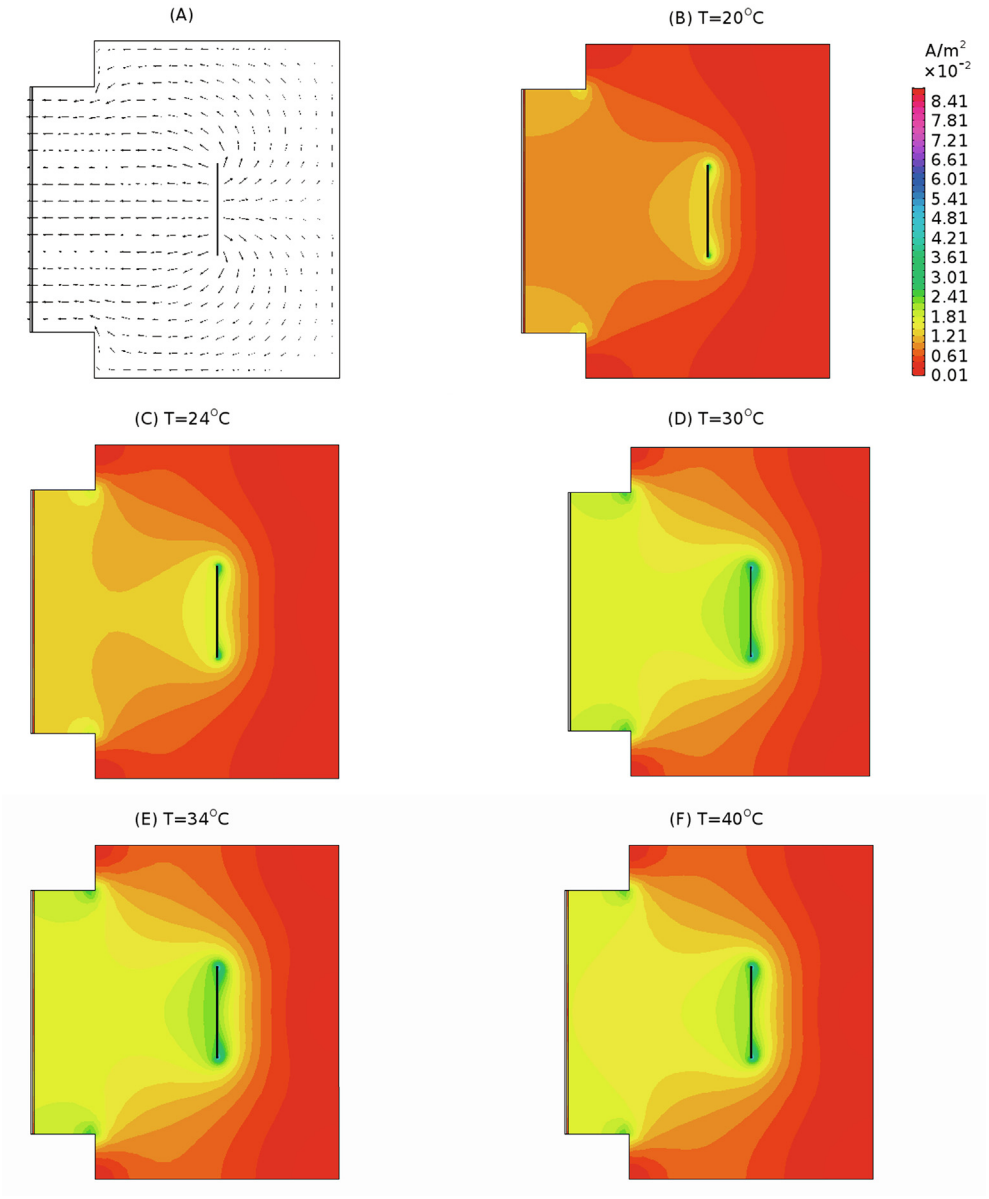

Fig. 5. Electrolyte (ionic) current density vector field (A, arrow plot) in MFC chamber and current density distribution (B-F, contour plots) in MFCs for five different operating temperatures at 0.02 V.

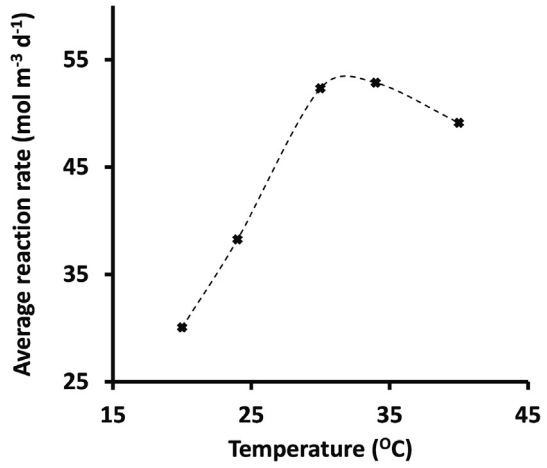

Fig. 6. Average reaction rate of oxidation in the biofilms as a function of operating temperature.

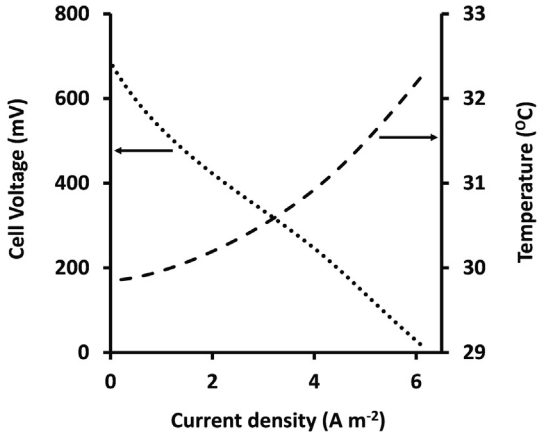

Fig. 7. Voltage (dotted line) and average cell temperature (dashed line) as a function of current density for MFC operating at 30 °C.

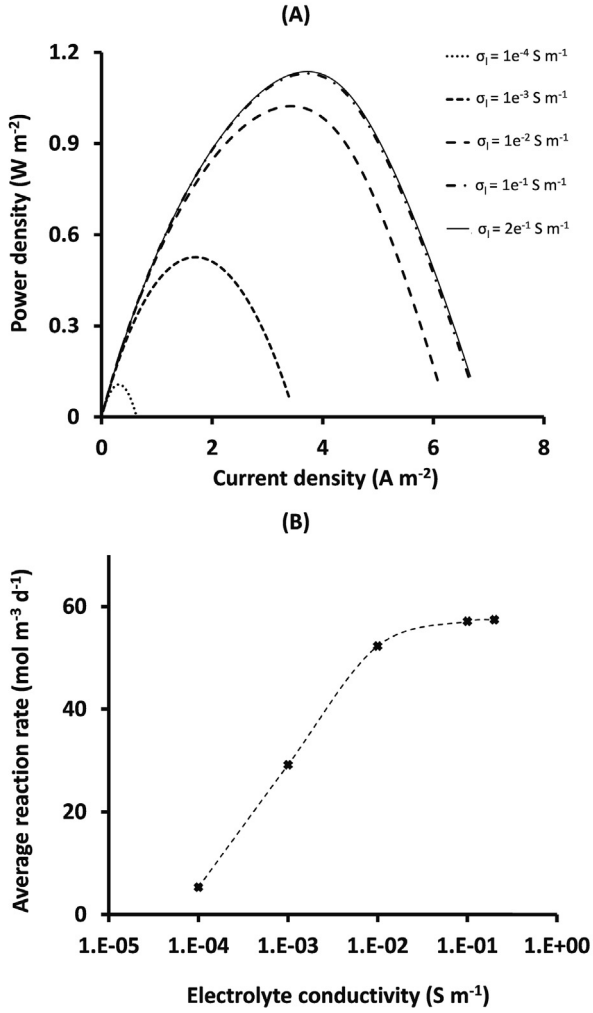

Fig. 8. (A) Polarization curves (power density vs current density) and (B) Average reaction rate of oxidation in the biofilms as a function of electrolyte conductivity.

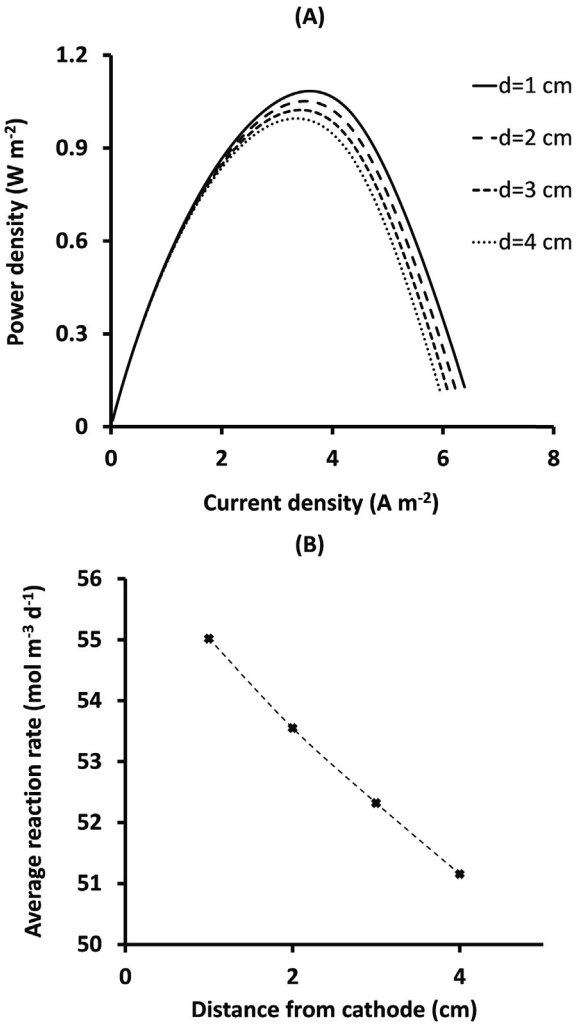

Fig. 9. (A) Polarization curves (power density vs current density) and (B) Average reaction rate of oxidation in the biofilms as a function of distance between two electrodes.

accordance with previous experimental and numerical studies [4,38,6,39] and is typically ascribed to the decrease in internal resistance as IED is decreased.

The effect of electrode spacing is also a strong function of the ionic strength of the solution. It was observed that when using electrolytes with higher conductivities ($\geqslant$0.01 S m^{-1}), decreasing the electrode spacing does not result in any significant gain in power output, but it does when the electrolyte conductivity is small ($\leqslant$0.001 S m^{-1}). For the result shown in Fig. 9A, the electrolyte conductivity was 0.01 S m^{-1} and we observed ~9% increase in power output on reduction of electrode spacing from 4 cm to 1 cm. However when an electrolyte with weak ionic strength (σ_l = 1e^{-4} S m^{-1}) is used, reducing the electrode spacing leads to ~130% increase in maximum power density.

It can also be seen from Fig. 9B that the average reaction rate is highest for d = 1 cm and decreases linearly with increase in IED. The lower internal resistance at d = 1 cm enables a higher electrode potential which thereby helps in improving the reaction rate of substrate oxidation in the biofilm. It should however be noted that very close positioning of the electrodes has been found to result in decreased performance due to oxygen contamination of the anode biofilm [40], and thus IED can only be decreased to a certain optimum distance before the trend is reversed.

4. Conclusion

The proposed steady state model successfully captures the effect of temperature on the MFC performance as observed from the experimental study. The 2D analysis allows us to visually represent and understand the changes in ionic and electronic current densities, and the local reaction rates in the two electrodes. This is one of the first attempts to numerically explain the non-linear performance trend with respect to temperature.

It is also shown that most of the parameters are inter-linked and it is imperative to account for these dependencies to obtain a realistic description of the MFC performance. The model proposed in this work is generic and can be applied to different MFC configurations. While the governing equations represented here for a steady state analysis, which allows for fast convergence and quick optimization, they can be easily modified to study the dynamic performance by including time dependence. It is also shown that the scope of the model is not limited to thermal analysis but can also be used for parametric studies and optimization of other system parameters. This applicability is highlighted by studying the effect of electrode spacing and ionic strength on the system performance, the results of which are in agreement with trends reported in literature.

Declaration of Competing Interest

The authors declare that they have no known competing financial interests or personal relationships that could have appeared to influence the work reported in this paper.

Acknowledgments

The authors would like to acknowledge the financial support by the Natural Environment Research Council (NERC) UK project grant: NE/R013306/1 and Engineering and Physical Sciences Research Council (EPSRC) UK project grant: EP/N009746/1.

Appendix A. Supplementary data

Supplementary data associated with this article can be found, in the online version, athttps://doi.org/10.1016/j.cej.2020.124176.

References

[1] Carlo Santoro, Catia Arbizzani, Benjamin Erable, Ioannis Ieropoulos, Microbial fuel cells: from fundamentals to applications. a review, J. Power Sources 356 (2017) 225–244.
[2] Jincheng Wei, Peng Liang, Xia Huang, Recent progress in electrodes for microbial fuel cells, Bioresour. Technol. 102 (20) (2011) 9335–9344.
[3] Xinyang Li, Guicheng Liu, Fujun Ma, Shaobin Sun, Siyu Zhou, Ryanda Enggar Anugrah Ardhi, Joong Kee Lee, Hong Yao, Enhanced power generation in a single-chamber dynamic membrane microbial fuel cell using a nonstructural air-breathing activated carbon fiber felt cathode, Energy Convers. Manage. 172 (2018) 98–104.
[4] Hong Liu, Shaoan Cheng, Bruce E. Logan, Power generation in fed-batch microbial fuel cells as a function of ionic strength, temperature, and reactor configuration, Environ. Sci. Technol. 39 (14) (2005) 5488–5493.
[5] S. Gadkari, S. Gu, J. Sadhukhan, Towards automated design of bioelectrochemical systems: a comprehensive review of mathematical models, Chem. Eng. J. 343 (2018) 303–316.
[6] V.B. Oliveira, M. Simões, L.F. Melo, A.M.F.R. Pinto, Overview on the developments of microbial fuel cells, Biochem. Eng. J. 73 (2013) 53–64, https://doi.org/10.1016/j.bej.2013.01.012 ISSN 1369-703X.http://www.sciencedirect.com/science/article/pii/S1369703X13000235.
[7] Jhuma Sadhukhan, Jon R. Lloyd, Keith Scott, Giuliano C. Premier, H. Yu Eileen, Tom Curtis, Ian M. Head, A critical review of integration analysis of microbial electrosynthesis (mes) systems with waste biorefineries for the production of biofuel and chemical from reuse of co_2, Renewable Sustain. Energy Rev. 56 (2016) 116–132.
[8] Sara Mateo, Pablo Cañizares, Francisco Jesus Fernandez-Morales, Manuel A. Rodrigo, A critical view of microbial fuel cells: What is the next stage? ChemSusChem 11 (24) (2018) 4183–4192.
[9] Shuiliang Chen, Sunil A. Patil, Robert Keith Brown, Uwe Schröder, Strategies for optimizing the power output of microbial fuel cells: Transitioning from fundamental studies to practical implementation, Appl. Energy 233 (2019) 15–28.
[10] Parisa Nouri, Ghasem Najafpour Darzi, Impacts of process parameters optimization on the performance of the annular single chamber microbial fuel cell in wastewater treatment, Eng. Life Sci. 17 (5) (2017) 545–551.
[11] Hyunsoo Moon, In Seop Chang, Byung Hong Kim, Continuous electricity production from artificial wastewater using a mediator-less microbial fuel cell, Bioresour. Technol. 97 (4) (2006) 621–627.
[12] Y. Feng, X. Wang, B.E. Logan, H. Lee, Brewery wastewater treatment using air-cathode microbial fuel cells, Appl. Microbiol. Biotechnol. 78 (5) (2008) 873–880.
[13] Sunil A. Patil, Falk Harnisch, Balasaheb Kapadnis, Uwe Schröder, Electroactive mixed culture biofilms in microbial bioelectrochemical systems: the role of temperature for biofilm formation and performance, Biosens. Bioelectron. 26 (2) (2010) 803–808, https://doi.org/10.1016/j.bios.2010.06.019 ISSN 0956-5663.http://www.sciencedirect.com/science/article/pii/S0956566310003209.
[14] Booki Min, Óscar Benito Román, Irini Angelidaki, Importance of temperature and anodic medium composition on microbial fuel cell (mfc) performance, Biotechnol. Lett 30 (7) (2008) 1213–1218.
[15] Mirella Di Lorenzo, Tom P Curtis, Ian M Head, Keith Scott, A single-chamber microbial fuel cell as a biosensor for wastewaters, Water Res. 43 (13) (2009) 3145–3154.
[16] A. Larrosa-Guerrero, K. Scott, I.M. Head, F. Mateo, A. Ginesta, C. Godinez, Effect of temperature on the performance of microbial fuel cells, Fuel 89 (12) (2010) 3985–3994.
[17] L.H. Li, Y.M. Sun, Z.H. Yuan, X.Y. Kong, Y. Li, Effect of temperature change on power generation of microbial fuel cell, Environ. Technol. 34 (13–14) (2013) 1929–1934.
[18] E.S. Heidrich, J. Dolfing, M.J. Wade, W.T. Sloan, C. Quince, T.P. Curtis, Temperature, inocula and substrate: contrasting electroactive consortia, diversity and performance in microbial fuel cells, Bioelectrochemistry 119 (2018) 43–50.
[19] S. Gadkari, M. Shemfe, J. Sadhukhan, Microbial fuel cells: a fast converging dynamic model for assessing system performance based on bioanode kinetics, Int. J. Hydrogen Energy 44 (29) (2019) 15377–15386.
[20] Mobolaji Shemfe, Siddharth Gadkari, Yu. Eileen, Shahid Rasul, Keith Scott, Ian M. Head, Sai Gu, Jhuma Sadhukhan, Life cycle, techno-economic and dynamic simulation assessment of bioelectrochemical systems: a case of formic acid synthesis, Bioresour. Technol. 255 (2018) 39–49.
[21] Mobolaji Shemfe, Siddharth Gadkari, Jhuma Sadhukhan, Social hotspot analysis and trade policy implications of the use of bioelectrochemical systems for resource recovery from wastewater, Sustainability 10 (9) (2018) 3193.
[22] Siddharth Gadkari, J. Mobolaji Shemfe, S. Annie Modestra, Venkata Mohan, Jhuma Sadhukhan, Understanding the interdependence of operating parameters in microbial electrosynthesis: a numerical investigation, Phys. Chem. Chem. Phys. 21 (2019) 10761–10772.
[23] V.M. Ortiz-Martínez, M.J. Salar-García, A.P. de los Ríos, F.J. Hernández-Fernández, J.A. Egea, L.J. Lozano, Developments in microbial fuel cell modeling, Chem. Eng. J. 271 (2015) 50–60.
[24] V.B. Oliveira, M. Simões, L.F. Melo, A.M.F.R. Pinto, A 1d mathematical model for a microbial fuel cell, Energy 61 (2013) 463–471.
[25] Jean-Marie Fontmorin, Junxian Hou, Shahid Rasul, Yu. Eileen, Stainless steel-based materials for energy generation and storage in bioelectrochemical systems applications, ECS Trans. 85 (13) (2018) 1181–1192.
[26] Dorin-Mirel Popescu, An investigation of bacterial composition and biofilm structure in mixed-community bioanodes, Newcastle University, 2016 [[Ph.D. thesis]].
[27] A.K. Marcus, C.I. Torres, B.E. Rittmann, Conduction-based modeling of the biofilm anode of a microbial fuel cell, Biotechnol. Bioeng. 98 (6) (2007) 1171–1182.
[28] Wen-Fang Cai, Jia-Feng Geng, Pu. Kai-Bo, Qian Ma, Deng-Wei Jing, Yun-Hai Wang, Qing-Yun Chen, Hong Liu, Investigation of a two-dimensional model on microbial fuel cell with different biofilm porosities and external resistances, Chem. Eng. J. 333 (2018) 572–582.
[29] Siddharth Gadkari, Sai Gu, Jhuma Sadhukhan, Two-dimensional mathematical model of an air-cathode microbial fuel cell with graphite fiber brush anode, J. Power Sources 441 (2019) 227145, https://doi.org/10.1016/j.jpowsour.2019.227145 ISSN 0378-7753.http://www.sciencedirect.com/science/article/pii/S0378775319311383.
[30] Sen Yao, Ya-Ling He, Bing-Ye Song, Xiao-Yue Li, A two-dimensional, two-phase mass transport model for microbial fuel cells, Electrochim. Acta 212 (2016) 201–211.
[31] Yingzhi Zeng, Yeng Fung Choo, Byung-Hong Kim, Ping Wu, Modelling and simulation of two-chamber microbial fuel cell, J. Power Sources 195 (1) (2010) 79–89.
[32] R.J. Millington, J.P. Quirk, Permeability of porous solids, Trans. Faraday Soc. 57 (1961) 1200–1207.
[33] Siddharth Gadkari, Beatriz Fidalgo, Gu. Sai, Numerical investigation of microwave-assisted pyrolysis of lignin, Fuel Process. Technol. 156 (2017) 473–484.
[34] Shaoan Cheng, Bruce E. Logan, Increasing power generation for scaling up single-chamber air cathode microbial fuel cells, Bioresour. Technol. 102 (6) (2011) 4468–4473.
[35] Olivier Lefebvre, Zi Tan, Shailesh Kharkwal, How Y. Ng, Effect of increasing anodic nacl concentration on microbial fuel cell performance, Bioresour. Technol. 112 (2012) 336–340.
[36] Doug Aaron, Costas Tsouris, Choo Y Hamilton, Abhijeet P Borole, Assessment of the effects of flow rate and ionic strength on the performance of an air-cathode microbial fuel cell using electrochemical impedance spectroscopy, Energies 3 (4) (2010) 592–606.
[37] Yama Mohan, Debabrata Das, Effect of ionic strength, cation exchanger and inoculum age on the performance of microbial fuel cells, Int. J. Hydrogen Energy 34 (17) (2009) 7542–7546.
[38] Chi-Yuan Lee, Ya-Ni Huang, The effects of electrode spacing on the performance of microbial fuel cells under different substrate concentrations, Water Sci. Technol. 68 (9) (2013) 2028–2034.
[39] Sona Kazemi, Melissa Barazandegan, Madjid Mohseni, Khalid Fatih, Systematic study of separators in air-breathing flat-plate microbial fuel cells? part 2: numerical modeling, Energies 9 (2) (2016) 79.
[40] Jung Mi Moon, Sanath Kondaveeti, Tae Ho Lee, Young Chae Song, Booki Min, Minimum interspatial electrode spacing to optimize air-cathode microbial fuel cell operation with a membrane electrode assembly, Bioelectrochemistry 106 (2015) 263–267.